Comparative Analysis of Monostable and Bistable Energy Harvester working under Vortex Induced Vibration (VIV)

By

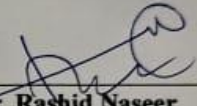Talha Bin Khalid

(Registration no.: 00000327291)
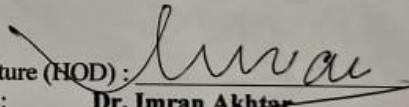
Supervisor: Dr Rashid Naseer

Department of Mechanical Engineering

College of Electrical and Mechanical Engineering

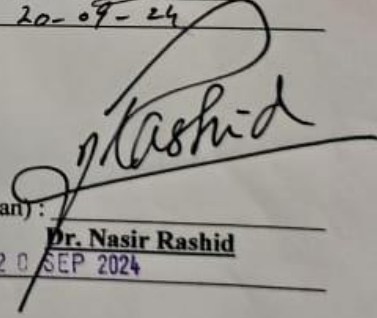National University of Sciences & Technology

Islamabad, Pakistan

(2024)

THESIS ACCEPTANCE CERTIFICATE

Certified that final copy of MS/MPhil thesis written by Mr. **NS Talha Bin Khalid**, Registration No. **00000327291** of **NUST College of E&ME** has been vetted by undersigned, found complete in all respects as per NUST Statutes/Regulations, is free of plagiarism, errors, and mistakes and is accepted as partial fulfillment for award of MS/MPhil degree. It is further certified that necessary amendments as pointed out by GEC members of the scholar have also been incorporated in the said thesis.

Signature: _____

Name of Supervisor: **Dr. Rashid Naseer**

Date: _____20-09-24_____

Signature (HOD): _____

Name: **Dr. Imran Akhtar**

Date: _____20-09-24_____

Signature (Dean): _____

Name: **Dr. Nasir Rashid**

Dated: _____20 SEP 2024_____

DEDICATION

To Dr. Rashid Naseer, whose motivation has a significant role in my master's.

This thesis is dedicated to my supervisor, Dr Rashid Naseer, who has provided tremendous direction, insight, and support throughout this journey.

I also like to thank the members of the Graduate Evaluation Committee (GEC) for their informative feedback and support.

I dedicate this work to my family, whose unwavering love and confidence in me have driven all my efforts. I also dedicate it to my friends, who consistently lifted my spirits and stood by me through challenges and triumphs. Your support made this achievement possible

ACKNOWLEDGMENT

First and foremost, I am extremely thankful for Allah Almighty's special blessings on me throughout my journey, without which I would never have achieved and accomplished what I have today.

I thank my advisor, Dr. Rashid Naseer, for his immense guidance, help, and support. I wouldn't be here today without his encouragement throughout all the stages of this research.

Moreover, I thank Dr Imran Akhtar, Dr Usama Bin Perwez, and Dr Abdul Rehman Mazhar for being on my thesis guidance and evaluation committee.

Finally, I would like to thank my parents, family members, family friends, and many other friends who have always been a constant source of adoration, support, and motivation for me.

ABSTRACT

An efficient, eco-friendly energy generation approach has increased the potential development of harvesting wind energy via a piezoelectric transduction mechanism, which can be a feasible replacement for conventional batteries in low-powered, portable, and wireless appliances and gadgets. Different phenomena harvest vibrational energy using wind, such as vortex-induced vibrations (VIV), wakegalloping, galloping, and flutter. These are dependent upon the form of the bluff body to be employed. Magnetic force enhances the performance of the energy harvester by non-linearity in the system as it will switch between mono-stable regions and bi-stable regions due to non-linear magnetic force; hence, there is a need to study this aspect. In this study, we compare the mono-stable variant and bi-stable variant of the piezo-aeroelastic energy harvester. The addition of base excitation to the system allows for additional research. Buckling is influenced by the non-linear force induced by a pair of magnets, which varies with their distance from one another. The efficiency analysis of both mono-stable regions and bi-stable regions is carried out on the magnetic separation at the equivalent coupled frequency for an accurate and effective comparison. The Euler-Lagrange technique has been used to develop a lumped parameter model. Non-linear magnetic force is shown in the equation by dipole dipole representation. The static frequency analysis and coupled frequency analysis are done using the mathematical model, after which a performance analysis is performed. The performance analysis is done by simulation using MATLAB. The study shows that bi-stability helps achieve broadband synchronization regions.

Keywords: Aeroelastic, Energy Harvesters, Vortex-Induced Vibrations (VIV), Mono-stable, Bi-stable, Non-linearities.

TABLE OF CONTENTS

LIST OF FIGURES

LIST OF TABLES

CHAPTER 1: INTRODUCTION

1.1 Research background:

The reduction and limitation of fuels for conventional energy generation has become a global concern. Attention has been shifted to generating energy through non-conventional techniques. Renewable energy, or "Green Energy," has grabbed much attention. Currently, energy generation is done using fossil fuels, i.e., coal, and nuclear. These methods affect the environment as radiation and harmful gases are released. Due to these concerns, scientists are trying to shift energy generation from conventional to non-conventional methods [1].

The growing concerns discussed above have forced us to focus on the invention of green energy generation by absorbing and transforming the green energy sources in our environment. The research has led to the invention of many energy generation sources such as biogas, vibrational, wind, wave & geothermal energies. Solar thermal and photovoltaic energy are two forms of solar energy that can be used [2, 3]. Large-scale production is needed to facilitate the electrical energy needs of the cities, for which wind energy and solar energy methods can be utilized. Solar photovoltaic energy methods are already commonly used nowadays. Every energy generation method has some limitations and drawbacks. Solar energy generation mainly depends on the weather, and it has a high maintenance cost, which is required after a regular timeframe, which makes it a little bit expensive [4, 5]. Solar thermal energy generation affects global warming and bird life, but wave energy generation has a high maintenance cost. Also, it affects marine life. Biogas energy generation in a large area is required, which has a high setup cost; wind turbines cannot be installed in a residential area as they require an adequate area for installation. While functioning, it creates noise pollution, and geothermal energy also contributes to global warming, a growing concern [6].

While exploring sustainable - environment-friendly, renewable (green) energy generation sources continues. A growing interest from researchers has developed regarding the use of ambient mechanical vibrational energy to generate electrical energy [7], which is the interest of this study. The battery pack used for different appliances has some concerns, such as regular condition checks, replacement, etc. Mechanical vibration energy generation systems can be used for low-power

generation. It can replace batteries for low-powered devices such as smart devices and wireless devices (wireless sensors, wireless networking systems & sensing networks).

1.2 Motivation

Recently, researchers in various fields have done a lot of research on converting mechanical vibrational energy to efficient electrical energy [8]. Energy harvesting has been a trending topic in the past 15 years due to the increasing energy demands. Converting ambient vibrations to efficient electricity is known as vibrational energy harvesting. Different modes of vibrations can result such as repetitive, spectral, or chaotic, and depending on the type of object, it can be observed in vibrations of different operational machinery, the vibration of the different bridges (wooden bridge, steel bridge, overhead bridge, suspension bridge), vibrations in building, structures (towers) due to earthquake, Flow-induced vibrations in ropes, string, wires, circular and rectangular poles, branches of tree, leaves of plants, and vibrations in human body while performing activities [9]. This ambient vibrational energy can be utilized through vibrational energy harvesters to provide power to self-powered gadgets [10], wireless sensors such as wildlife identity tags, pacemakers [11], pain relievers requiring low power, spinal simulators [12], sensors requiring low power used in marine, aerospace field and MEMS (Micro-Electrical-Mechanical Systems) [13, 14]. Compared to energy harvesters, batteries are cheap. Still, they have certain drawbacks such as they have a limited lifespan, after a particular time replacement is required which is costly, and after disposal, its waste is harmful to the environment [15, 16]. In addition to all these drawbacks, some locations involve special procedures for placing batteries, such as bridges, poles, etc.
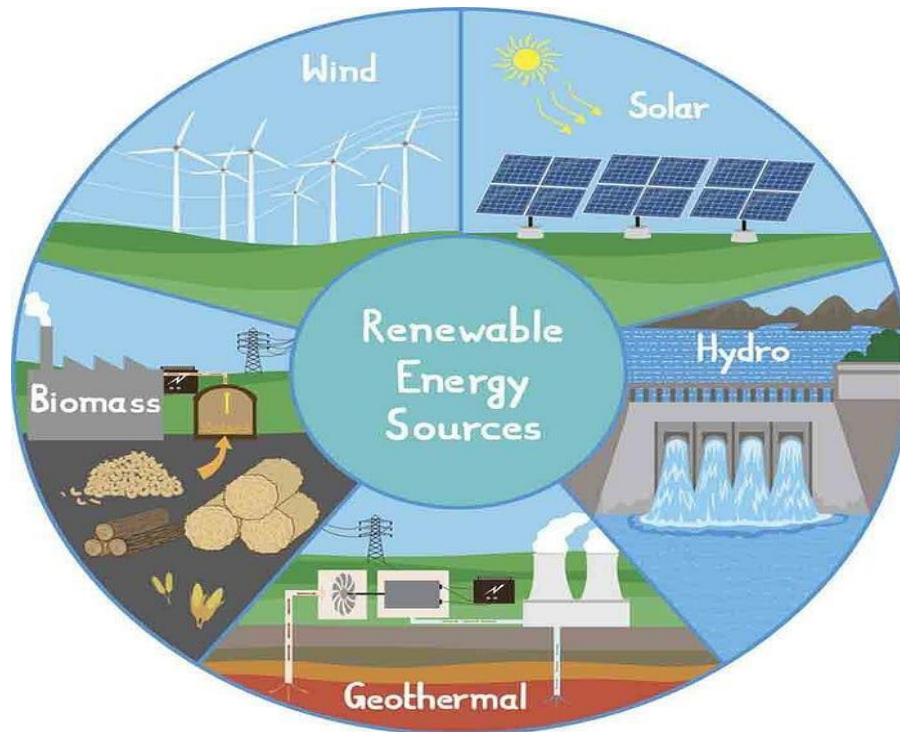
Figure 1.1: Different types of "Renewable Energy Sources" utilized for electrical energy generation.

Energy conversion requires a mechanism; mechanical vibrational energy is usually converted to electrical energy by applying transduction mechanisms such as electrostatic [17, 18], electromagnetic [19, 20], and piezoelectric [21, 22]. Piezoelectric transduction mechanism can be used in different modes; it is simple and easy to apply, due to which it is used most of the time as compared to other transduction mechanisms [23]; some other advantages of using piezoelectric transduction are ease of manufacturing [24], functional at a broad range of frequencies [25], ease of installation, small space required for installation [26]. Self-powered devices require low power; researchers agree that mechanical vibrational energy harvesters are the most feasible solution for self-powered devices [27, 28].

1.3 Research objectives

In the modern era, optimal and feasible solutions are recommended, such as mechanical vibration energy harvesting, an environment-friendly solution to minimize or eliminate the use of batteries for low-powered wireless devices. An efficient model must be designed and its performance analyzed. During the past ten years, vortex-induced vibrational energy harvesting has become a popular idea. There is an idea that vibrational energy harvesters can manufacture self-

3

powered gadgets. The issue with a vibrational energy harvester working on the phenomenon of vortex-induced vibration is that it is functioning efficiently only in its resonance region. In contrast, outside the region, the efficiency drops significantly. In this study our focus is to investigate the performance efficiency of energy harvesters having non-linear magnetic force, using VIV.

The vibrational energy harvester compromises a cantilever beam with a piezoelectric layer attached to either its upper or lower side, a bluff body attached to its free end, and another end fixed. We create a non-linear lumped parameter model based on the Euler-Lagrange beam theory. The mathematical model is used to collect performance data using various parameters through simulation. Subsequently, the outcomes are verified by comparing them with the published study articles.

1.4 Thesis outline

Chapter 1 is an introduction in which an explanation of renewable "green" energy generation methods is provided, which are feasible alternatives to conventional energy generation methods. Also, why is there a need for alternate energy generation methods? The last segment focuses on the feasibility and applications of mechanical vibration energy harvesters.

Chapter 2 overviews different transduction mechanisms used in energy harvesting methods, piezoelectric materials, and energy harvesting models based on aeroelastic instabilities. In addition, a literature review is done for a comprehensive review of various energy harvesters based on vibrational energy. The literature review gives us an overview of the research on improving the efficiency of vibrational energy harvesters in the last decade.

Chapter 3 is based on the mathematical modelling of a piezoelectric energy harvester with non-linear magnetic force and the development of a lumped parameter model. Eigenvalue problems are used for static analysis and frequency analysis.

Chapter 4 consists of results obtained by simulation, which involves varying the parameters to perform a performance analysis of the energy harvester when it is excited using the influence of VIV.

Chapter 5 compromises the conclusion, the investigation limitations, and future research directions.

CHAPTER 2: LITERATURE REVIEW

2.1 Mechanism for transforming vibration into electric current

Two significant developments should be noted when assessing the state of the art: developing energy harvesting and storage systems for small or microscopic devices and advancing methods for large-scale industrial applications. The latter trend, motivated by the need to power progressively smaller gadgets without connecting them to the electrical grid, encourages the development of energy-harvesting units for those devices. Batteries are used as the power source in these situations. However, the primary drawback of batteries is their short lifespan. When they run out, they have to be replenished, which can be expensive and complex depending on where they are. Innovative energy harvesting techniques now include utilizing kinetic energy and energy from the human body. Examples include capturing energy from human movements (such as walking or even during sleep), body heat, or heart contractions. Human motion, characterized by high amplitudes and low frequency, presents a unique challenge for designing miniature generators worn on the body. Nonetheless, several devices that utilize these methods have been developed, including a watch that uses body heat to power its mechanism and charge its battery.

- A ring with an integrated thermoelement that transforms body heat into the electric energy required to charge the battery [29].
- A heart pacemaker in which the heart's movement will power [30].

- One intriguing concept involves a shoe equipped with a generator. Research indicates that a person weighing 68 kg can generate 67J of energy while walking [31].
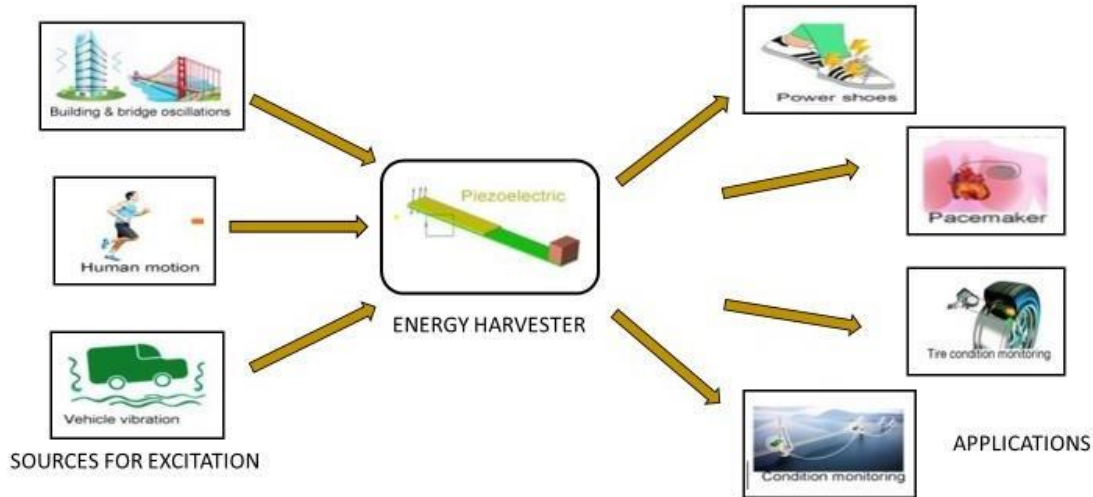
Figure 2.1: Sources of mechanical vibrations and their utilization in Appliances by using Piezoelectric Energy Harvester

Unfortunately, current devices designed for this purpose only recover a few millijoules of energy, limiting their ability to power larger devices. However, future advancements may expand the range of devices that can be powered this way, including mobile phones and portable computers.

Mechanical vibration is one of the most effective methods for energy harvesting. This process involves converting motion into electrical energy by linking a moving mechanism to a device capable of generating electricity. An energy harvesting device from vibration transforms kinetic energy into electrical energy. This technique allows for electricity generation from various deformations, such as piezoelectric materials or the movement of a magnet within a coil. Mechanical vibration power is typically sourced from the environment. The energy harvested from vibrations is converted into electrical energy and stored in batteries, for instance [32].

Currently, there are several methods available for capturing energy from vibrations. These methods include the electromagnetic, electrostatic, piezoelectric, and magnetostriction methods. Figure 2.2 illustrates the methods for harvesting energy from vibrations through different

mechanisms.
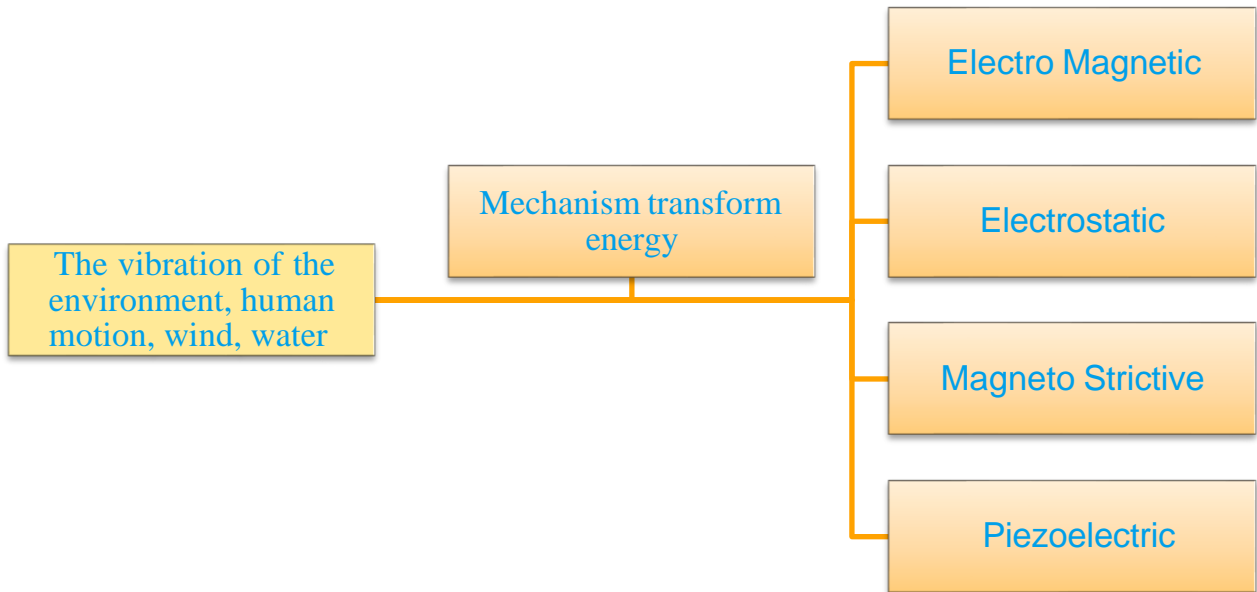
Figure 2 2: Mechanisms for conversion of vibrational energy to electrical energy

2.2 Utilizing piezoelectric material for energy harvesting

The piezoelectric method of energy harvesting has garnered significant attention recently. Research in this area aims to reduce the power consumption of small electronic devices, such as wireless sensors used for health monitoring. The primary objective is to provide a power supply for these devices by utilizing vibration energy from the environment.

Magneto-strictive materials, known for their high magnetic and mechanical coupling coefficients, offer another promising approach. These materials are advantageous due to their high flexibility and Curie temperature. When applied, mechanical forces induce flexible tension that changes the magnetic field intensity. High-capacity capacitors, energy regulators, and converters are the standard components of devices that harvest energy utilizing magneto-strictive materials.

Using the electromagnetic approach, electrical power is produced by utilizing the kinetic energy of a vibrating mass. There are two types of states for electromagnetic energy collecting devices: reverse and standard. A moving magnet produces a magnetic field, whereas in the usual setup, the

coil stays fixed. In the opposite arrangement, the coil vibrates while the magnet remains fixed.
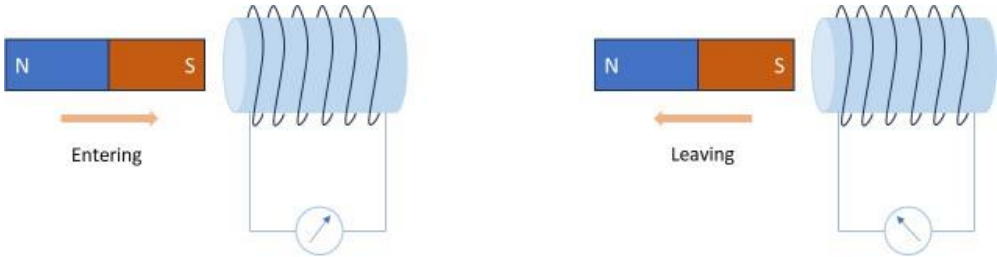
Figure 2.3: Illustration of Electromagnetic transduction mechanism

With the help of a variable condenser polarised by electrets—dielectrics that produce an ongoing external electric field in a manner akin to permanent magnets—the electrostatic approach transforms the kinetic energy of vibrations into electrical energy. A dielectric substance that moves in between two wires separates them in an electrostatic generator. The piezoelectric approach is more versatile than the electrostatic method, despite its widespread use..[33]
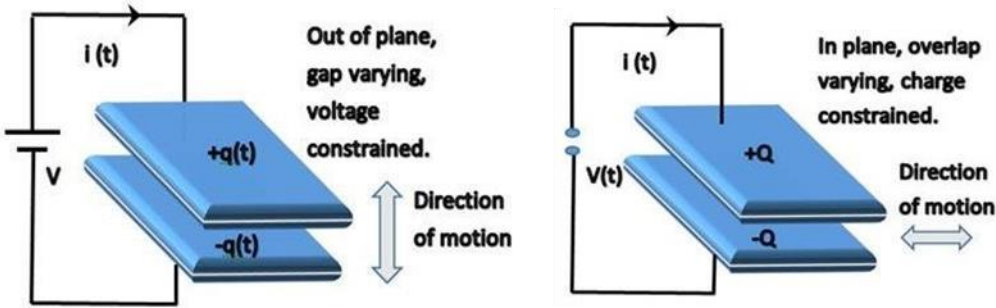
Figure 2.4: Electrostatic transduction mechanism

Since the discovery of ferroelectric materials like barium titanate (BaTiO3) and lead zirconate titanate (PZT), researchers have continuously developed various synthetic piezoelectric materials with diverse electromechanical, mechanical, and thermal properties. This section highlights several high-performance piezoelectric materials and reviews different transducer states for piezoelectric energy harvesting. Additionally, it provides an overview of standard mathematical models and conditioning circuitry.

2.3 Piezoelectric materials

Numerous piezoelectric materials have been produced in the last century, with perovskite lead zirconate titanate (PZT) being the most widely used. Niobium or lanthanum doping of PZT, a polycrystalline monolithic piezoelectric ceramic, is used to produce soft and hard piezoelectric materials, respectively. Since they can create high voltages (50 V to 100 V) and have direct coupling, which allows for operation without bias voltages, piezoceramics, like PZT, are frequently utilised in sensors and actuators. But normally, the currents are quite low (ranging from nanoamp to milliamp). But PZT contains lead, which has led to continuous research into novel formulations.

As an example, the researcher created a PNN-PZT ceramic that has a coupling coefficient that is noticeably higher than that of traditional PZT ceramics. Piezoelectric ceramics have a high density and are fragile, despite being inexpensive and having good coupling. PZT thin films have been produced for flexibility to solve these challenges, particularly in microelectromechanical systems (MEMS), and techniques including grain texturing and epitaxial thin films on substrates have been used to increase coupling. The main areas of ongoing study are improving electrode texturing, investigating substitute substrate materials, creating lower-temperature production techniques, and optimising material deposition for 3D transducers.

For hydrostatic sensors, such active and passive SONAR systems, porous piezoelectric materials show higher hydrostatic piezoelectric strain and voltage coefficients than dense piezoelectric materials. Furthermore, although having a somewhat lower coupling than ceramics, piezoelectric polymers, such as polyvinylidene fluoride (PVDF), have been created to offer lightweight and flexible substitutes. While some studies increased PVDF coupling by raising the β phase percentage in the material composition using a phase-inversion approach, the researcher's efforts

to create PVDF utilising near-field electrospinning methods intended to raise the coupling coefficient.

Figure 2.5: Piezoelectric Materials

Beyond PZT and PVDF, piezoelectric energy-harvesting transducer materials can be categorised into five groups: piezoelectric single crystals, lead-free piezoelectric, high-temperature piezoelectric, piezoelectric nanocomposites, and piezoelectric foams [34].
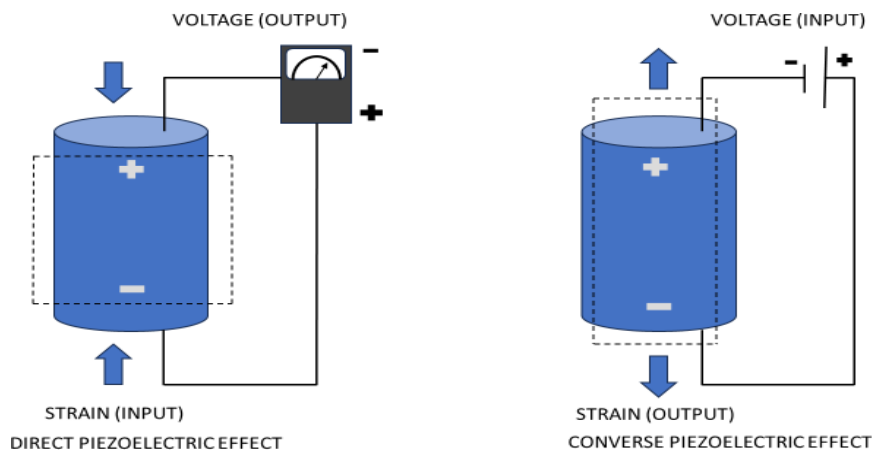
Figure 2.6: Illustration of Piezoelectric transduction mechanism

2.4 Energy harvesting through aeroelastic vibrations using piezoelectricity

When exposed to wind, a structure can exhibit several types of aerodynamic responses, including fluttering, VIV, galloping, and buffeting. These responses can involve complex phenomena such as bifurcations, limit-cycle oscillations, internal resonances, and chaotic motions. The system's behaviour is influenced by factors such as the geometry of the beam, its stiffness, the characteristics of the fluid, system nonlinearity, and aerodynamic effects. Typically, nonlinear analysis is used to predict these responses.

Researchers in civil, architectural, and aerospace engineering focus on reducing or controlling these vibrations to minimize potential damage. However, the same aerodynamic instabilities that cause issues can also be harnessed for energy collection. This section explores various aerodynamic instabilities and their potential for energy harvesting.
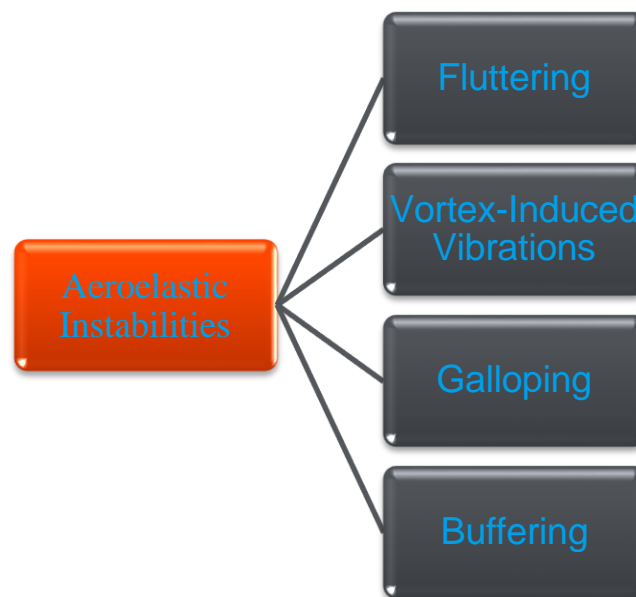
Figure 2.7: Different types of aeroelastic instabilities

2.4.1 Flapping in Airfoil Sections

Flutter is a type of aerodynamic instability that occurs when wind impacts an airfoil or aeroplane wing, and the wind speed exceeds a critical threshold determined by design parameters. This happens because the damping provided by the structure is insufficient to counteract the motions

induced by aerodynamic forces. Flutter is similar to galloping in terms of its physics, but it differs as galloping involves a single degree of freedom. In contrast, flutter involves multiple degrees of freedom and typically produces less power for the same-sized structure. Fluttering was among the first aeroelastic phenomena investigated for energy storage [35].

Figure 2.8: Schematic of (Airfoil) flutter-based piezoelectric energy harvester

2.4.2 Vortex-Induced Vibrations in Circular Cylinders

When fluid flows over a circular cylinder, it generates a series of vortices shed from the trailing edge. If the frequency of these vortices aligns with one of the system's fundamental frequencies, significant oscillations, or synchronization, can occur. The mechanism of vortex-induced oscillation relies on resonance and remains stable only within a narrow range of incoming flow velocities and Strouhal numbers. Outside this range, the efficiency of energy conversion drops. Modelling VIV can be complex due to the absence of pressure information in computational fluid dynamics approaches. A reduced-order model often balances computational efficiency with accuracy [36, 37].
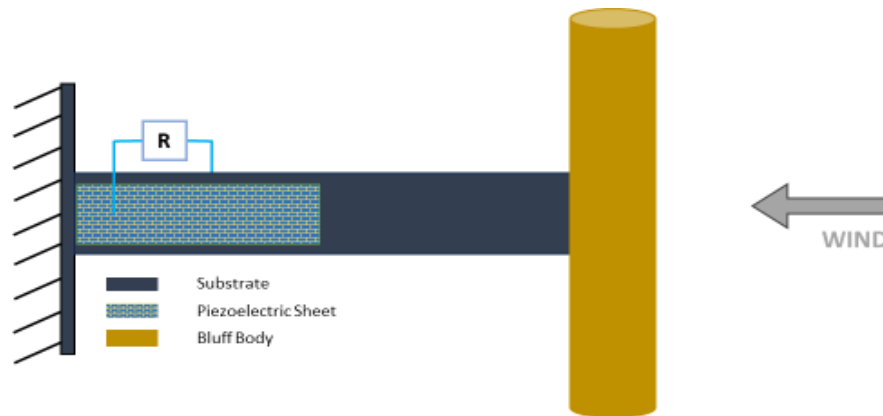
Figure 2.9: Schematic of (Cylindrical body-based) Vortex induced vibrations (VIV) based piezoelectric energy harvester

2.4.3 Galloping Energy Harvesters

Galloping refers to high-amplitude oscillations seen in prismatic cylinders with flat cross-sections when the flow velocity exceeds a critical value. Various cross-sectional shapes, such as D-section, triangular, rectangular, and square, can capture energy from these oscillations. Galloping typically occurs in a plane perpendicular to the incoming flow and is often called transverse galloping. It happens when the derivative of the steady-state aerodynamic lift coefficient becomes negative, as per Den Hartog's condition for galloping. Galloping-based energy harvesters effectively collect energy from steady, uniform flow patterns [38].
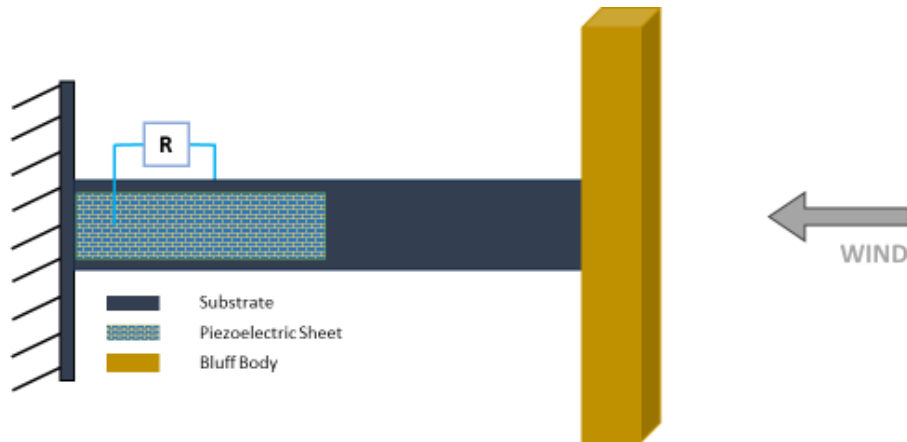
Figure 2.10: Schematic of Galloping-based piezoelectric energy harvester

2.4.4 Wake Galloping Energy Harvesters

Wake galloping occurs when multiple cylinders are placed in series. The vortices influence the oscillations in one cylinder shed from the preceding cylinder. This phenomenon is highly dependent on the displacement and diameters of the cylinders and occurs at specific distances between them.
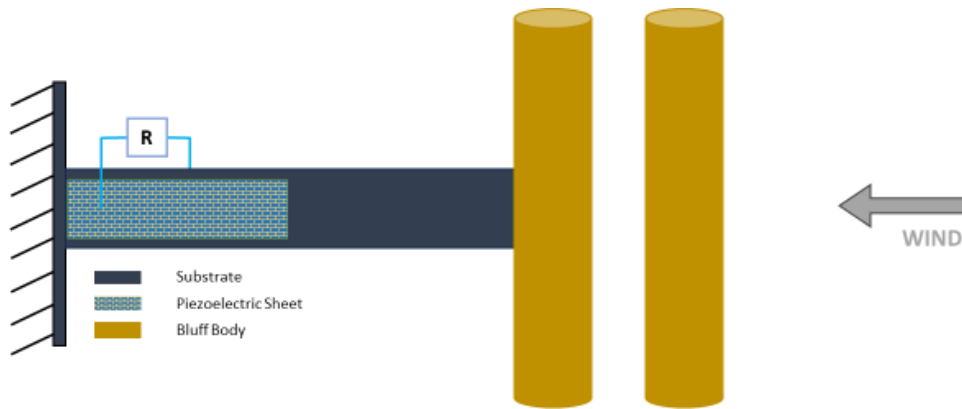
Figure 2 11: Schematic of Wake-Galloping based piezoelectric energy harvester

Mechanical vibrational energy is a promising source of energy that can be converted into electrical power. Piezoelectric energy harvesting has gained significant attention for its ability to convert

mechanical energy into electrical power without requiring external voltage sources, magnetic fields, or interactions like electromagnetic, triboelectric, and electrostatic effects. This relies solely on the material's internal polarization [39].

2.5 Recent research

Recent studies have explored various energy harvesting methods based on aerodynamic instabilities:

Galloping phenomena: Research has demonstrated that piezoelectric harvesters based on galloping can be highly effective at low wind speeds. Studies have investigated different designs, including tip masses with D-shaped cross-sections and continuously rotating bluff bodies.
Researchers have also examined the effects of ambient load representations on galloping-based harvesters and explored ways to enhance energy density and efficiency.
Investigated the potential of piezoelectric materials for recharging batteries by comparing two types: the macro-fiber composite (MFC) actuator and the monolithic piezoceramic material PZT. Key points include:
MFC Actuator
•   Utilizes piezo fibers and interdigitated electrodes.
•   Has a higher g33 piezoelectric coupling coefficient, resulting in more significant strain and force production compared to monolithic PZT.
•   Attractive for power harvesting due to its mechanical properties.
Efficiency Comparison
•   The MFC and PZT's efficiency in generating electrical energy was assessed.
•   MFC was less effective for power harvesting due to low current generation.
Battery Charging Capability
•   MFC was ineffective for battery charging because of its insufficient current output.
•   PZT successfully charged various nickel-metal hydride batteries.
•   The study determined the maximum battery capacity that PZT could efficiently charge
[40][41].
Vortex-Induced Vibrations:
•   VIV energy harvesting has gained momentum due to its renewable and clean nature. When

the Reynolds number (Re) surpasses the critical value of approximately 47 for flow around a fixed

circular cylinder, vortex shedding occurs, potentially leading to VIV if the cylinder is elastically supported.

• This phenomenon is relevant across various engineering domains, including wind, ocean, and bridge engineering. The concept of harnessing VIV for energy was advanced with the VIV Aquatic Clean Energy (VIVACE) converter, designed to capture energy from water currents. Further exploration was conducted on the performance of the VIVACE converter at high Reynolds numbers.

• Vortex-induced vibration (VIV) energy harvesting has become popular due to its renewable nature. When the Reynolds number exceeds 47, vortex shedding can occur around a fixed cylinder, leading to VIV if the cylinder is elastically supported. This phenomenon is essential in wind, ocean, and bridge engineering. The VIV Aquatic Clean Energy (VIVACE) converter was developed to harness energy from water currents, with further studies exploring its performance at high Reynolds numbers.

• To improve performance, the combination of VIV with galloping-based harvesters has been explored. Researchers have studied different bluff body shapes and states to optimize energy harvesting.

Nonlinear approaches and additional magnetic forces have extended the resonance range and enhanced efficiency [42][43].

Flutter:

• Energy harvesting from flutter has been researched with designs such as thin rectangular plates and piezoelectric sheets. Studies focused on optimizing these designs for improved efficiency and stability. Innovations in dynamic adjustment systems for flutter harvesters have been explored to enhance device stability and application range.

• Adding a beam stiffener effectively enhances the power generation capabilities of aeroelastic energy harvesters based on galloping, vortex-induced vibration (VIV), and flutter.

This modification can increase maximum power output by more than tenfold, with comparable or smaller displacement, thereby not exacerbating fatigue issues. For VIV-based harvesters, the lock-in region has also been expanded. Among these, the flutter-based harvester shows the highest efficiency and can operate across a wide range of wind speeds. The VIV-based harvester best suits environments with stable and low wind speeds. In contrast, the galloping-based harvester is

recommended for conditions with solid wind flows due to its superior power output at high wind speeds [44][45].

Wake-Galloping:

•	This phenomenon has been investigated for its potential in energy harvesting, with designs incorporating piezoelectric cantilever beams and fixed cylinders. Research has focused on creating oscillating vortices to drive energy generation.

•	The proposed aeroelastic metastructure effectively addresses vibration suppression and energy harvesting through aerodynamic galloping and base excitations. The study examines two states:

•	State I involves regular locally resonating masses with no external forces.

State II, which adds bluff bodies to these masses, making them susceptible to aerodynamic galloping forces. Piezoelectric electromechanical coupling is integrated into the local resonators to convert mechanical and electrical energy. An aero-electro-mechanical model was formulated using a lumped parameter approach for a finite metastructure chain. Numerical parametric studies were performed to optimize the metastructure's performance [46].

While these studies show promise, each method has limitations. Galloping and fluttering can be less effective at higher wind speeds, while wake galloping is less efficient when wind speeds are low. Due to their resonant properties, VIV are effective at lower wind speeds. Further research is needed to refine these technologies and improve their efficiency under various conditions.

2.6 Research gap

Even though there has been a lot of research on energy harvesters based on VIV, there is still a limitation, as energy harvesting is only significant in small synchronization regions. A recent study noted that increasing wind speed decreases power generation. To avoid this limitation, researchers have been working on broadband energy harvesting devices, which require initial excitation such as flow-induced vibration or base excitation [47, 48]. The power generation efficiency of the energy harvester needs improvement for which different design and techniques [49, 50], mechanical modulation systems [51, 52], surface optimization, the addition of pair of magnets for multistability [53,54,55], base excitation, [56,57] and forces generated by external sources [58,59].

There is much ongoing research based on the output of energy harvesters by variation of ambient wind speed. However, this study analyzes the effect of non-linear magnetic force in mono-stable states and bi-stable states using the influence of VIV. The impact of different parameters on the performance of energy harvesters is studied using varying parameters. The system's insights can be gathered by analyzing the results gathered in the mono-stable states and bi-stable states.

CHAPTER 3: MATHEMATICAL MODELLING OF PIEZOELECTRIC ENERGY HARVESTER USING VORTEX-INDUCED VIBRATIONS (VIV)

3.1 Introduction

In this chapter, the modelled energy harvester is shown. The piezo-aeroelastic energy harvester using VIV is explained. The basic model of the energy harvester consists of a cantilever beam and a piezoelectric layer attached to the upper side of a cantilever beam; on the free end, a bluff body is connected while the other end is fixed. For qualitative and quantitative analysis, a distributed parameter model is used; however, in this study, we only require qualitative analysis, for which a lumped parameter model is developed. The system is modelled based on a simple mass-spring system, as shown in Figure 3.1. The static frequency analysis is used to find the magnetic separations at which buckling would occur. The effect of non-linear magnetic force represented by the dipole-dipole model is analyzed using the lumped parameter model. Using the Euler-Lagrange equation, the equations of motion are developed.
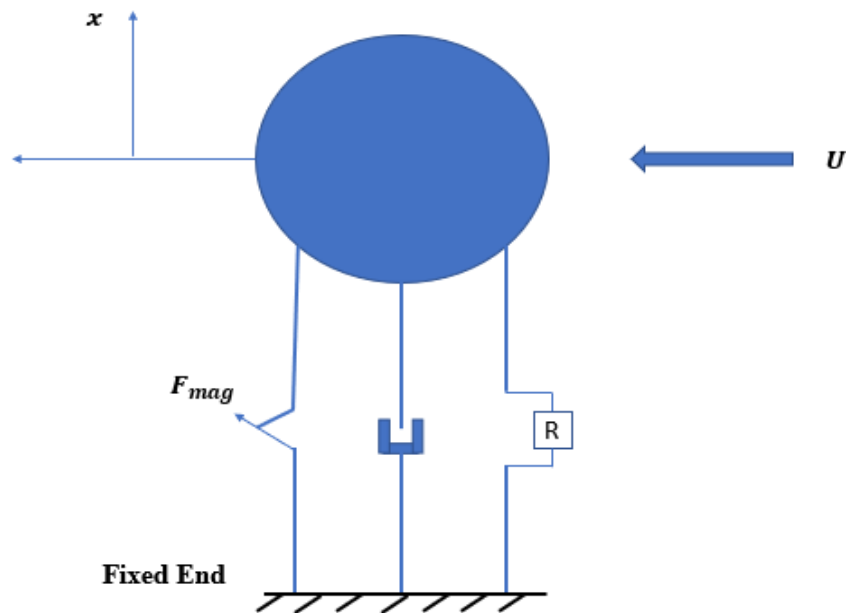
Figure 3. 1: Schematic of the spring-mass-damper representation of piezoelectric energy harvester working under VIV

3.2 Description of the model

Figure 3.3 shows the piezoelectric energy harvester designed for this study. Figure 3.2 shows that the cantilever is made of anamorph material, a cylindrical body attached to its free end. Electrodes surround the sides of the piezoelectric layer. An electrical load is connected to the electrodes, represented by load resistance "R." The electrodes are fragile as they should be thoroughly conducted while covering the utilized piezoelectric layer.

The system has four fixed symmetric magnets incorporated in it; the purpose of these magnets is to increase the efficiency of the piezo-aeroelastic energy harvester. Two pairs of magnets are placed, as the ones on the right are attached to the cylindrical bluff body, while the ones on the left are attached to a support without attachment to the beam. The magnets will affect the piezoelectric energy harvester as they will attract to a specific extent (distance between magnets) when the beam buckles on both sides. The parameters are denoted as piezoelectric layer length from fixed end L_p, beam length from fixed end L_t, and length of cylindrical bluff body L.. The beam can buckle because of an axially compressive force, which occurs when the distance between magnets drops to a particular value. Two magnetic forces result from the pair of magnets, but for our simplicity, they are combined into one. As we change the distance between magnets, the effects of magnetic force on the system change. The mono-stable state and bi-stable state are linked by adjusting the separation between magnets; this is utilized to compare the system's performance in both states.

Table 3.1: Parameters of Suggested Piezoelectric Energy Harvester

Description	Units	Parameter	Value
Mass of the cylindrical bluff body	kg	M	0.05
The diameter of the cylindrical bluff body	m	D	0.05
Length of the cylindrical bluff body	m	L	0.2
Experimental Constant	-	A	12
Experimental Constant	-	B	0.24
Damping Ratio	-	ξ	0.003
Density of Air	kg/m^3	p (rho)	1.225
Distance between magnets	m	d_m	0.011 to 0.04
Effective magnetic moments	-	a_1 , a_2	0.2
Electromechanical coupling coefficient	N/V	Θ	1.55 x 10^3
Capacitance	F	C_p	120 x 10^{-9}
Natural Frequency	Hz	ω_n	10
Strouhal number	-	S	0.116
Steady lift coefficient	-	C_L	0.3
Mean drag coefficient	-	C_d	1.2
Load resistance	Ω	R	10^6
Permeability constant	NA^{-2}	μ	4π x 10^{-7}
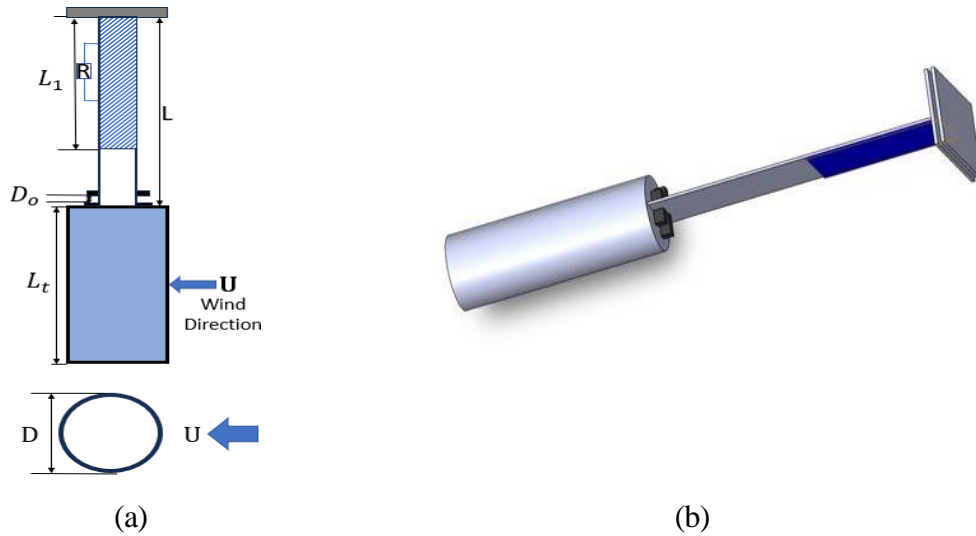
(a)   (b)
Figure 3. 2: Proposed model for Piezoelectric energy harvester

3.3 Developing the equation of motion for the model

The extended Hamilton principle will be utilized to formulate the equations of motion for the system. The extended Hamilton principle is written as

$$\int_{t_1}^{t_2} (\delta T - \delta U + \delta W)dt = 0 \tag{1}$$

$t_2 \sim t_1$ is any period, W is the amount of non-conservative work completed, T is the kinetic energy, and U is potential energy. The kinetic energy of the model is shown as

$$T = \frac{1}{2}\int_0^{L_p} m_1 \left[\frac{\partial z(x,t)}{\partial t}\right]^2 dx + \frac{1}{2}\int_{L_p}^{L_T} m_2 \left[\frac{\partial z(x,t)}{\partial t}\right]^2 dx + \frac{1}{2}M_C \left[\frac{\partial z(x,t)}{\partial t}\bigg|_{x=L_T} + L_C \frac{\partial^2 z(x,t)}{\partial x \partial t}\bigg|_{x=L_T}\right]^2 dx$$

$$+ \frac{1}{2}I_T \left[\frac{\partial^2 z(x,t)}{\partial x \partial t}\bigg|_{x=L_T}\right]^2 \tag{2}$$

M_C is the tip mass, I_T is the moment of inertia while masses m_1 and m_2 are defined by their region such as:

$$0 \leq x \leq L_p \Rightarrow m_1 = b_1\rho_s h_s + b_2\rho_p h_p$$

$$L_p \leq x \leq L_T \Rightarrow m_2 = b_1\rho_s h_s \tag{3}$$

The non-linear term can be expressed as non-linear potential energy, which is non-linear potential force, such as in μ is the permeability constant, described as $4\pi 10^{-7} NA^{-2}$ in this model we will use it as non-linear potential energy. The potential energy expression would be

$$U = \frac{1}{2}\int_0^{L_T} [EI_1 z'(x,t)_2]dx + \frac{1}{2}\int_{L_p}^{L_T} [EI_2 z'(x,t)_2]dx - \frac{1}{2}\int_0^{L_p} e_{31}b_2(y_1 + y_2)z'(x,t)V(t)dx$$

$$- \frac{1}{2}\frac{\varepsilon_{33}b_2 L_p}{h_p}V^2(t) + \frac{\mu a_1 a_2}{2\pi}\left(\frac{\partial^2 z(x,t)}{\partial x^2}\bigg|_{x=L_T} + d_m^2\right)^{\frac{3}{2}} \tag{4}$$

e_{31} is the coefficient of stress, ε_{33} is the permittivity constant, a_1 and a_2 are magnetic moments while d_m is the separation between pair of magnets seen in Figure 3.3.

While functioning, the system has effects of dissipative load resistance losses, viscous damping,

23

and vortex-induced vibration force, which results in non-conservative workdone. It is written as

$$\delta W_{nc} = -R\dot{Q}\delta Q - \int_0^{L_T} \left| c_v \frac{\partial z(x,t)}{\partial t} \right| \partial z(x,t)dx \tag{5}$$

For simplicity, the electrode voltage by using Ohm's law can be expressed as

$$V(t) = R\frac{dQ}{dt} \tag{6}$$

By the addition of simplified terms in the expression for the extended Hamilton principle, the equations of motion will give

$$EI\frac{\partial^4 z(x,t)}{\partial x^4} + c\frac{\partial z(x,t)}{\partial t} + m\frac{\partial^2 z(x,t)}{\partial t^2} - e_{31}\frac{(y_1 + y_2)}{2}b_2 V(t)\left(\frac{d\delta(x)}{dx} - \frac{d\delta(x - L_p)}{\delta x}\right) = 0 \tag{7}$$

$$-e_{31}\,(y_1 + y_2)\,b_2\int_0^{L}\partial^3 z(x,t)\,dx - \varepsilon_{33}\,b_2\,L_p\,\frac{dV(t)}{dt} = \frac{V(t)}{R} \tag{8}$$

For simplicity, the equations of motion can be expressed as:

$$m\ddot{x}(t) + 2m\xi\omega_n x(t) + m\omega_n^2 x - \theta V + \frac{dU_{mag}}{dx} = F_{viv} \tag{9}$$

$$C_p V + \frac{V}{R} + \theta x = 0 \tag{10}$$

The kinetic energy is T, and the potential energy is U. The modified oscillator van der Pol model was explored and developed by Facchinetti et al. [60]. Afterwards, the wake oscillator model's representation was verified by Violette et al. [61]. The numerical forecast displayed in the modified van der Pol oscillator model and the experimental measurement by Alkaydin et al. [62] agreed well.

The fluctuating lift force, which the modified van der Pol model describes as m's potential energy and W is the non-conservative work done, is directly proportional to the circular body acceleration. The modified van der Pol model written as

$$q(t) + \beta\omega_s\left(q^2 - 1\right)q + \omega_s^2 q = \frac{A}{D}x \tag{11}$$

ω_s is the vortex shedding frequency expression $\omega_s = 2\pi SUD^{-1}$. β is the experimental constant, U is the velocity of fluid flow, and S shows Strouhal number.

The modified van der Pol model's lift coefficient can be expressed as $C_L = 0.5q(t)C_{L0}$. This expression can be utilized to get an expression of aerodynamic lift force [63].

$$F_{viv} = \frac{\rho U^2 DL}{2} \cdot \frac{C_{L0}}{2}q - \frac{\rho UDL}{2}C_d x \tag{12}$$

Rho "ρ" is density of fluid which in our case is air, D is diameter of cylinder, L is length of cylinder, and C_{L0} and C_d are the mean lift and drag coefficients.

Finally, the equations of motion can be expressed as

$$m\ddot{x}(t) + 2m\xi\omega_n\dot{x}(t) + m\omega_n^2 x - \theta V - \frac{3x\mu a_1 a_2}{2\pi(x^2 + d_m^2)^{\frac{5}{2}}} = \frac{\rho U^2 DL}{2} \cdot \frac{C_{L0}}{2}q - \frac{\rho UDL}{2}C_d\dot{x} \tag{13}$$

$$C_p V + \frac{V}{R} + \theta x = 0 \tag{14}$$

$$q(t) + \beta\omega_s(q^2 - 1)q + \omega_s^2 q = \frac{A}{D}x \tag{15}$$

As per [64], three different types of analysis were performed. We will discuss two of them in this chapter; the third is mentioned in the results and discussion chapter.

3.4 Static analysis (finding the bifurcation point):

The static analysis determines the effect of the magnetic separation on the system's state. It establishes a critical magnetic spacing where the system transitions from mono-stable to bi-stable behaviour. The static position x_s as a function of magnetic spacing dm can be derived from the modified fundamental frequency equation and the mechanical properties.

If the magnetic spacing exceeds the critical value $d_{m.cr}$, the system remains in a mono-stable state. Below this critical value, it transitions to a bi-stable state.

26

The magnetic spacing is minimized to a specific limit upon which the system will buckle. This buckling will result in two stable solutions in the mono-stable state and a solution showing instability in the bi-stable state. Neglecting the force due to VIV, polarization, and terms dependent on time present in the equation, we get the expression for static equilibrium as

$$m\omega_n^2 x_s - \frac{3x_s K_m}{(x_s^2 + d_m^2)^{\frac{5}{2}}} = 0 \tag{16}$$

The values of parameters are mentioned in **Error! Reference source not found.**. Utilizing the p arameters, we have plotted Figure 3.3. This figure shows the plot of static displacement x_s of the system concerning the magnetic spacing between a pair of magnets $d_{m.cr}$. The results show that the specific magnetic distance is the critical magnetic separation $d_{m.cr}$. This shows the bifurcation point as, at this point, the system equilibrium changes. If $d_m < d_{m.cr}$ then bi-stable equilibrium in which the system is unstable while if $d_m > d_{m.cr}$ then mono-stable equilibrium in which all values of x_s are zero. As the magnetic separation between a pair of magnets decreases, there is an increase in the values of static equilibrium in the bi-stable region.
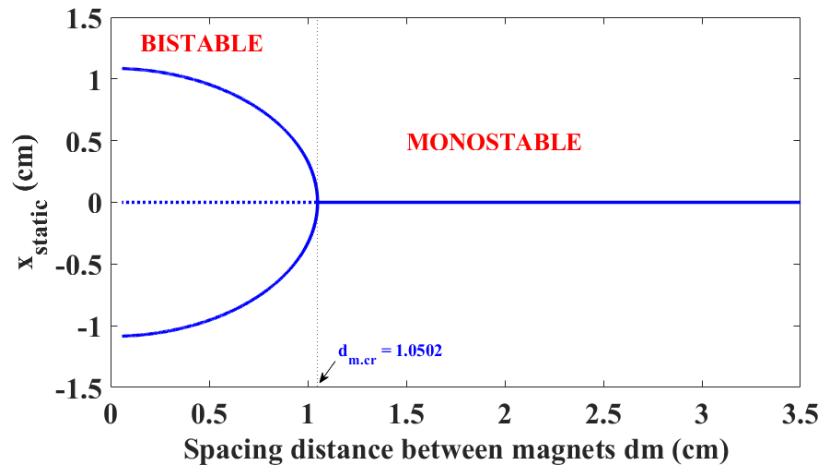
Figure 3.3: Effect on static displacement by variation in magnetic spacing between magnets

3.5 Coupled frequency analysis:

This analysis investigates how the spacing between magnets affects the system's fundamental frequency.

To find the response of natural frequency for the piezo magnetoelastic system in mono-stable state and bi-stable state, we induct the variable y, which is written as

$$y = x - x_s \tag{17}$$

$$x = x_s + y \tag{18}$$

When the equation of motion for undamped and unforced is substituted for x, it gets

$$\ddot{y} + \omega_n^2 y + \omega_n^2 x_s + \frac{3K_m}{m} \frac{(x_s + y)}{((x_s + y)^2 + d_m^2)^{2.5}} = 0 \tag{19}$$

Applying the Taylor series for the non-linear term in Eq. 19.

$$\ddot{y} + \omega_n^2 y + \omega_n^2 x_s - \frac{1}{m} \frac{3K_m x_s}{(x_s^2 + d_m^2)^{2.5}} + \frac{y}{m} \left\{ \frac{15K_m x_s^2}{(x_s^2 + d_m^2)^{3.5}} - \frac{3K_m}{(x_s^2 + d_m^2)^{2.5}} \right\} = 0 \tag{20}$$

If Static equilibrium expression is utilized, we will get the expression as

$$\ddot{y} + \left(\omega_n^2 + \frac{1}{m} \left\{ \frac{15K_m x_s^2}{(x_s^2 + d_m^2)^{3.5}} - \frac{3K_m}{(x_s^2 + d_m^2)^{2.5}} \right\} \right) y = 0 \tag{21}$$

From Eq. 16, we get the expression for modified fundamental frequency as

$$\omega_c = \left(\omega_n^2 + \frac{1}{m} \left\{ \frac{15K_m x_s^2}{(x_s^2 + d_m^2)^{3.5}} - \frac{3K_m}{(x_s^2 + d_m^2)^{2.5}} \right\} \right)^{\frac{1}{2}} = 0 \tag{22}$$

Decreasing the magnetic separation reduces the fundamental frequency, shifting the resonant frequencies to lower values and allowing the harvester to operate effectively at lower wind speeds. This is represented in Figure 3.4.

The static displacement of the system influences the modified fundamental frequency. The system's behavior is shown in Figure 3.4; the modified fundamental frequency is plotted against the magnetic separation by using Eq. 22. Decreasing the magnetic separation reduces the fundamental frequency to a value $d_{m.cr}$, which shows the buckling point. Fundamental frequency increases as the magnetic separation is decreased $d_m = 1.0502\ cm$ after the buckling point $d_{m.cr}$.
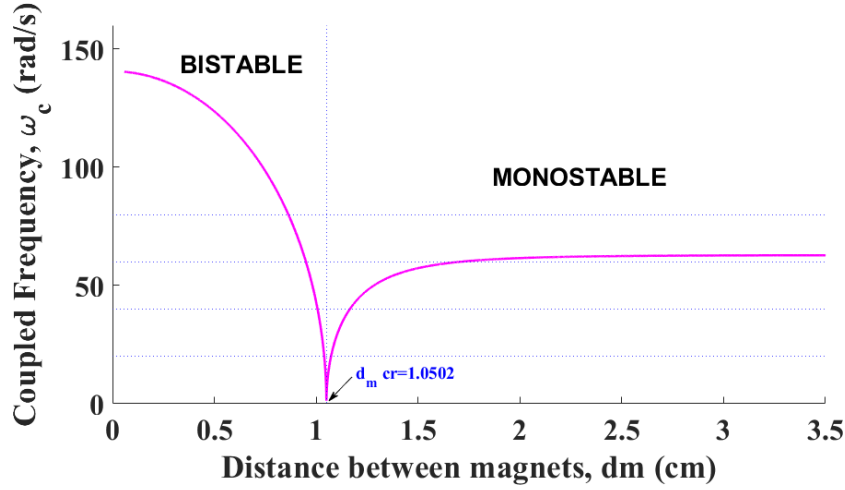
Figure 3.4: Coupled Frequency with variation in magnetic spacing between magnets

3.6 State Space Representation

The linear coupled governing equations Eq. 13 to Eq. 15 can be numerically solved using state space representation. State variables represent the state of a system at a given time; for example, in any system, they may represent the position, velocity, and acceleration. It helps view the behavior of the dynamic of the system [65]. The introduction of the state space variable converts linear Eq. 13 to Eq. 15 into first-order differential equations. Which can be written as

$$\dot{y}_1 = y_2 \tag{233}$$

$$y_2 = -\omega_c^2 y_1 - \left(2\xi\omega_n + \frac{F_2}{m}\right) y_2 + \frac{\theta}{m} V + \frac{F_1}{m} q_1 \qquad \text{Eq. 24}$$

$$V = -\frac{\theta}{C_p} y_2 - \frac{1}{RC_p} V \qquad \text{Eq. 255}$$

$$\dot{q}_1 = q_2 \qquad \text{Eq. 266}$$

$$q_2 = -\alpha\omega_c^2 y_1 - \left(2\alpha\xi\omega_n + \alpha\frac{F_2}{m}\right) y_2 + \alpha\frac{\theta}{m} V + \left(\alpha\frac{F_1}{m} - \omega_s^2\right) q_1 + \beta\omega_s q_2 \qquad \text{Eq. 277}$$

$$\alpha = \frac{A}{D}, F_1 = \frac{\rho U^2 DL}{2} \cdot \frac{C_L}{2}, F_2 = \frac{\rho UDL}{2} C_d$$

In matrix form, the Eq. 23, Eq. 24, Eq. 25, Eq. 26 and Eq. 27 are written as

29

$$
\begin{pmatrix} \dot{y}_1 \\ y_2 \\ V \\ q_1 \\ q_2 \end{pmatrix} =
\begin{pmatrix}
0 & 1 & 0 & 0 & 0 \\
-\omega_c^2 & -2\omega_n - \dfrac{F_2}{m} & \dfrac{\theta}{m} & \dfrac{F_1}{m} & 0 \\
0 & -\dfrac{\theta}{C_p} & \dfrac{-1}{RC_p} & 0 & 0 \\
0 & 0 & 0 & 0 & 1 \\
-\alpha\omega_c^2 & -2\alpha\xi\omega_n - \alpha\dfrac{F_2}{m} & \dfrac{\alpha\theta}{m} & -\omega_s^2 + \alpha\dfrac{F_1}{m} & \beta\omega_s
\end{pmatrix}
\begin{pmatrix} y_1 \\ y_2 \\ V \\ q_1 \\ q_2 \end{pmatrix}
\qquad \text{Eq. 28}
$$

3.7 Effect of load resistance on coupled frequency by variation of magnetic spacing

Figure 3.5 illustrates the relationship between coupled frequency and load resistance at various magnetic spacings (d_m). The linked frequency follows a flat trend across 10^2 to 10^8 ohms of load resistance, with deviations from 10^5 to the fifth ohms to 10^6 ohms.

For smaller values of dm, such as $d_m=0.86$ and $d_m=0.94$, the coupled frequency generally remains constant at lower frequencies (20-40 rad/s), with increases as the load resistance climbs beyond 10^5 ohms up till 10^6 ohms. As dm increases, notably at $d_m=1.7$ and $d_m=1.153$, the frequency swings upwards, stabilising at higher frequencies, around 80 rad/s, but with low change in response to increased load resistance.

The trends show that higher magnetic spacings (d_m) correspond to higher coupled frequencies, whereas the coupled frequency is relatively insensitive to changes in load resistance, regardless of the dm value. This indicates that as the magnetic spacing rises, the system becomes less responsive to load resistance while the coupled frequency remains relatively steady.
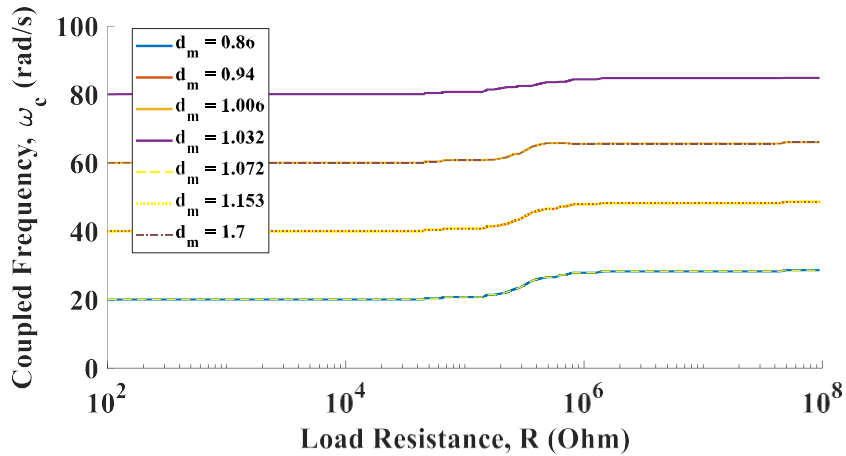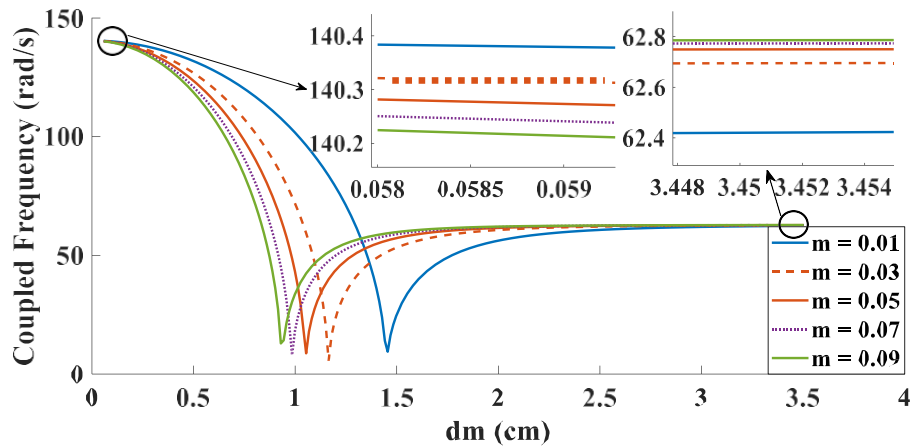
Figure 3.5: Coupled frequency analysis with varying load resistance at different magnetic spacings

3.8 Effect of mass on the coupled frequency with variation in the magnetic spacing

Figure 3.6 depicts the relationship between coupled frequency (in rad/s) and mass change, designated by m, for various dm values (in cm). As mass "m" goes from 0.01 to 0.09, the coupled frequency has a discernible trend. For lower values of m (e.g., m = 0.01), the coupled frequency begins high and decreases abruptly as dm increases, hitting a minimum before gradually rising. As m grows, the intensity of the dip reduces, and the minimum frequency shifts slightly to the right, becoming less noticeable. Higher values of m (e.g., m = 0.09) result in a significantly flatter frequency curve, showing less sensitivity to changes.

Figure 3.6: Effect of mass on the coupled frequency with the varying magnetic spacing between magnets

3.9 Analyze the effect of magnetic spacing on potential energy with variation in the magnetic spacing

In Figure 3.7, For both mono-stable and bi-stable setups, the dynamic behaviour of the system is investigated at the same coupled frequency. It is evident that the potential energy for dm = 1.7 cm, 1.153 cm, and 1.072 cm has a lowest potential energy at x = 0. In contrast, there are two stable sites where the potential energy is minimum when the dm is dropped to dm = 1.032 cm, 1.006 cm, 0.94 cm, and 0.886 cm. This indicates that the system has changed the distance between the magnets, going from a mono-stable to a bi-stable area. As was demonstrated in the previous section, load resistance has an impact on the coupled damping ratio, which the performance analysis will also take account of.

32
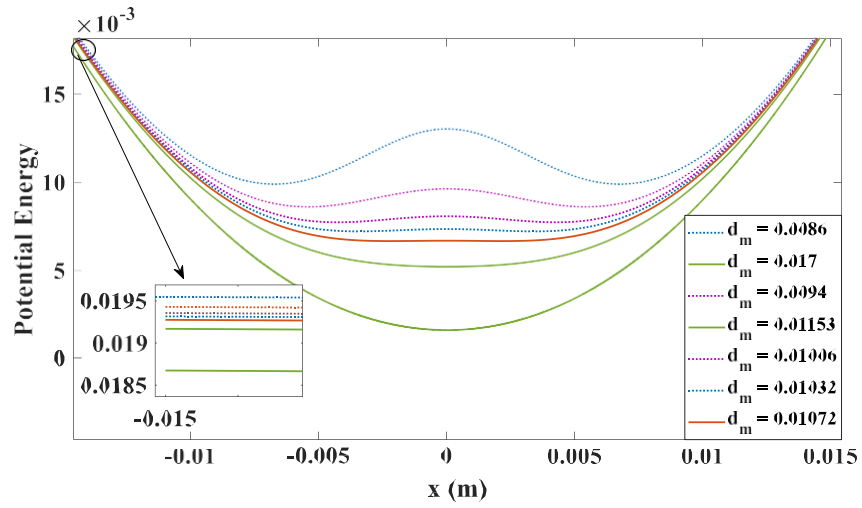
Figure 3.7: Potential energy variation with displacement of the system at different magnetic spacings between magnets

CHAPTER 4: RESULTS AND DISCUSSION

4.1 Non-linear Dynamic Analysis:

The nonlinear dynamic analysis examines the dynamic response under various magnetic spacings and electrical load resistances. The coupled equations of motion are solved numerically.

Lower magnetic spacings decrease the resonant wind speeds, making the system more effective at lower flow velocities. With reduced spacing, the synchronization region becomes narrower, and the displacement amplitude decreases. Optimal electrical load resistance maximizes the harvested power. The performance is best at a resistance level that depends on the system.

Therefore, the region with a sharp increase in global frequency corresponds to the range of load resistances with relatively large electromechanical damping. This is accurate for both setups. Outside of this area, both designs have almost constant global frequencies and small damping coefficients. This linear analysis clarifies how the load resistance influences the electromechanical damping variations and the commencement of the synchronisation area.

To enable a more comprehensive comparison between bi-stable and mono-stable energy harvester arrangements, parameter values are selected to maintain the same coupled frequency in each scenario. Four samples are defined with selected values at the same coupled frequency, as given in Table 4.1 and shown in Figure 3.5.

Table 4.1: Distance between pair of magnets for same coupled frequency

	Coupled Frequency (rad/sec)	Spacing between the pair of magnets (cm)	
		Mono-stable region	Bi-stable region
Case:1	20rad/sec	1.072	1.032
Case:2	40rad/sec	1.153	1.006
Case:3	60rad/sec	1.7	0.94
Case:4	80rad/sec	-	0.86

For instance, when the connected frequency equals 20 rad/s, the energy harvester can function in two states: mono-stable (magnetic spacing: 1.072 cm) and bi-stable (magnetic spacing: 1.032 cm).

Since the nonlinear axial force is changed while keeping all other parameters constant, it is particularly useful to visualize the state shift from a mono-stable state to a bi-stable state as a function of magnetic spacing. The mono-stable condition is attained with a magnetic separation of 1.153cm at a coupled frequency of 40rad/s, and the bi-stable state is reached at a magnetic spacing of 1.006cm. Another position is chosen where, for the linked frequency of 80rad/s, the mono-stable state has no magnetic magnetic spacing, and the bi-stable state has a magnetic spacing of 0.86 cm.

4.2 Analysis at coupled frequency 20rad/sec

In Table 4.1 (a) (d_m = 1.072 cm), the average harvested power peaks at a wind speed of around 2.6 m/s. The average captured power is roughly 0.07 W. The power rapidly decreases back to zero after rising steeply with wind speed, peaking at about 2.6 m/s. This has a narrow, sharp peak. The average gathered power peaks at a substantially lower value in Table 4.1 (b) (d_m = 1.032 cm) at about 3.5×10^{-3} W, at a lower wind speed of about 1.7 m/s. In comparison to Table 4.1 (a), Table 4.1 (b) shows a more steady increase in power with wind speed and a broader peak, indicating that power stays reasonably high across a longer range of wind speeds before gradually declining.

(a)   (b)
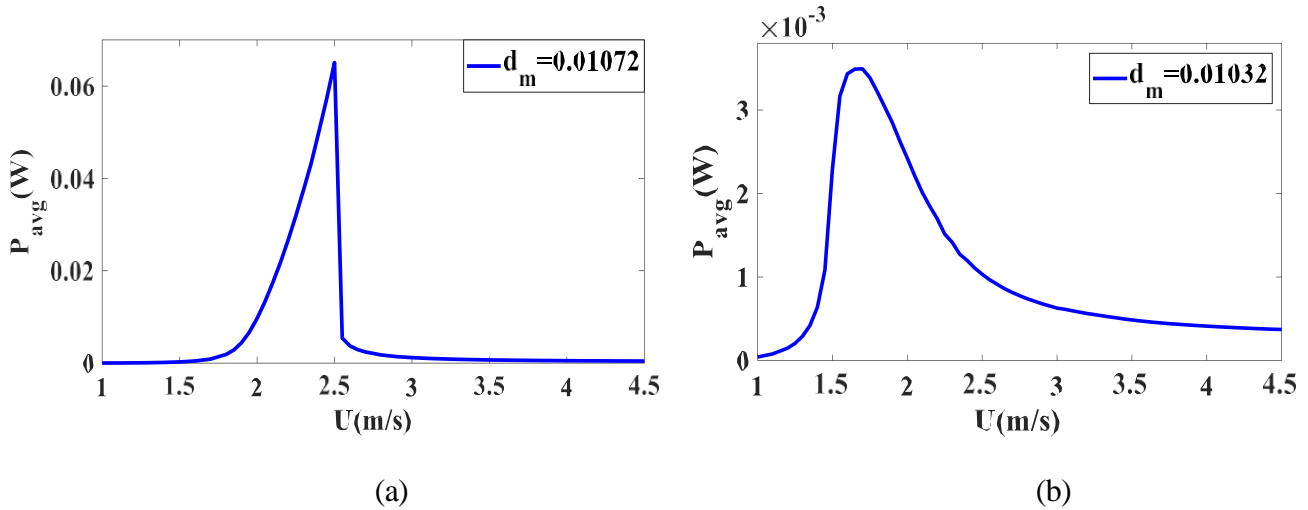
Figure 4.1: Average harvested power at (a) d_m=1.072cm (mono-stable) (b) d_m=1.032cm (bi-stable)

4.3 Analysis at coupled frequency 40 rad/sec

The average gathered power reaches its maximum in Figure 4.2: (a) (d_m = 1.153 cm) at a wind speed of about 3.4 m/s, or 0.45 W. The average gathered power reaches its maximum value in Figure 4.2: (b) (d_m = 1.006 cm) at a wind speed of roughly 2.3 m/s, or 0.014 W. At 5.7 m/s, a second, lesser peak with a value of about 0.005 W emerges. As wind speed climbs beyond 3.4 m/s,

the gathered power in Figure 4.2: (a) rapidly drops to zero. The harvested power rises fast with rising wind speed. The peak is distinct and pointy. There is a dual-peak behaviour in Figure 4.2: (b). At approximately 2.3 m/s for the first peak and 5.7 m/s for the second, there are two peaks. This indicates that the system can harvest power at two different wind speed ranges for $d_m = 1.006$ cm. However, the total power production is significantly less than that of Figure 4.2: (a). The system in Figure 4.2: (a) is successful within a limited wind speed range (around 3.2 to 3.6 m/s) and mostly operates around a single peak. Although the total power harvested is minimal, there is some power harvested over a wider range of wind speeds in Figure 4.2: (b), where two maxima occur at separate wind speeds (2.3 m/s and 5.7 m/s).

(a)   (b)
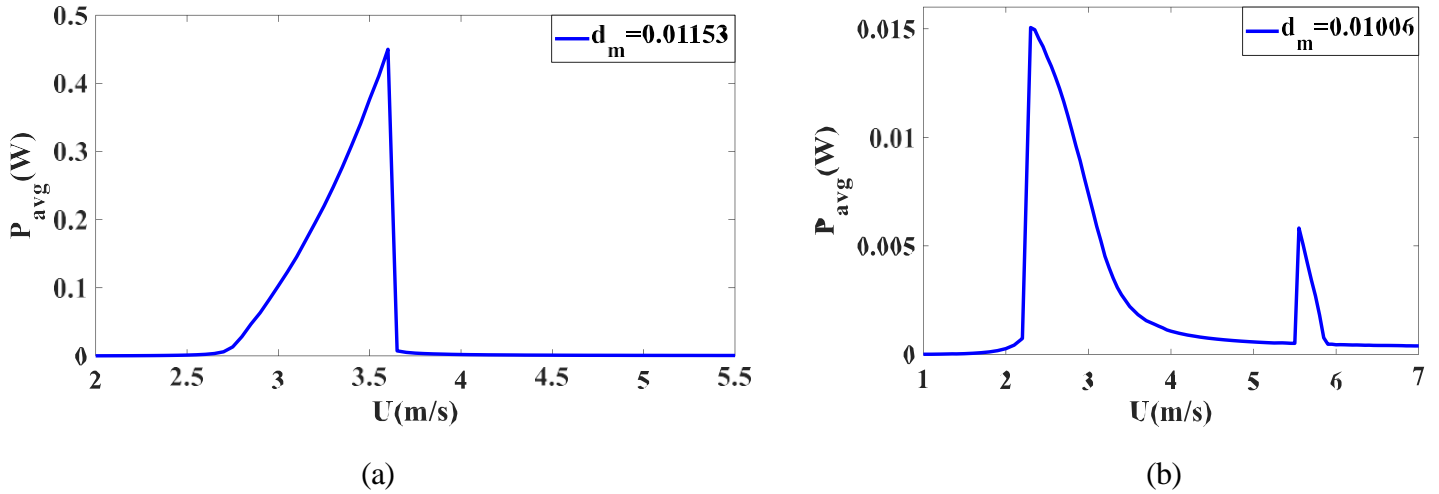
Figure 4.2: Average harvested power at (a) d_m=1.153cm (mono-stable) (b)d_m=1.006cm (bi-stable)

4.4 Analysis at coupled frequency 60 rad/sec

The average gathered power reaches its maximal value in Figure 4.3 (a) ($d_m = 1.7$ cm, mono-stable) at a wind speed of around 5 m/s, or roughly 2.3 W. The average gathered power reaches a much lower peak value in Figure 4.4 (b), with $d_m = 0.94$ cm, bi-stable, at approximately 0.09 W, at a wind speed of approximately 4.5 m/s. In the power curve, there are other, smaller peaks, especially around 8 m/s with a value of roughly 0.04 W. The gathered power in Figure 4.5 (a) increases gradually as wind speed increases, peaking at 5 m/s before suddenly falling to zero. A single, big peak spans a constrained range of wind speeds in this graph. The power swings substantially and has many peaks in Figure 4.6 (b). Around 4.5 m/s is the first major peak, and 8 m/s is the second one. Even though the total power is far less than in Figure 4.7 (a), this indicates

36

that the system has more complicated, bi-stable behaviour and can capture power across a wider range of wind speeds. The system in Figure 4.8 (a) focusses on a single, distinct peak and functions within a limited wind speed range of around 4.5 m/s to 5 m/s. Though the total amount of power captured is substantially less in Figure 4.9 (b), it is distributed over a wider range of wind speeds (from 4 to 10 m/s) with many peaks.

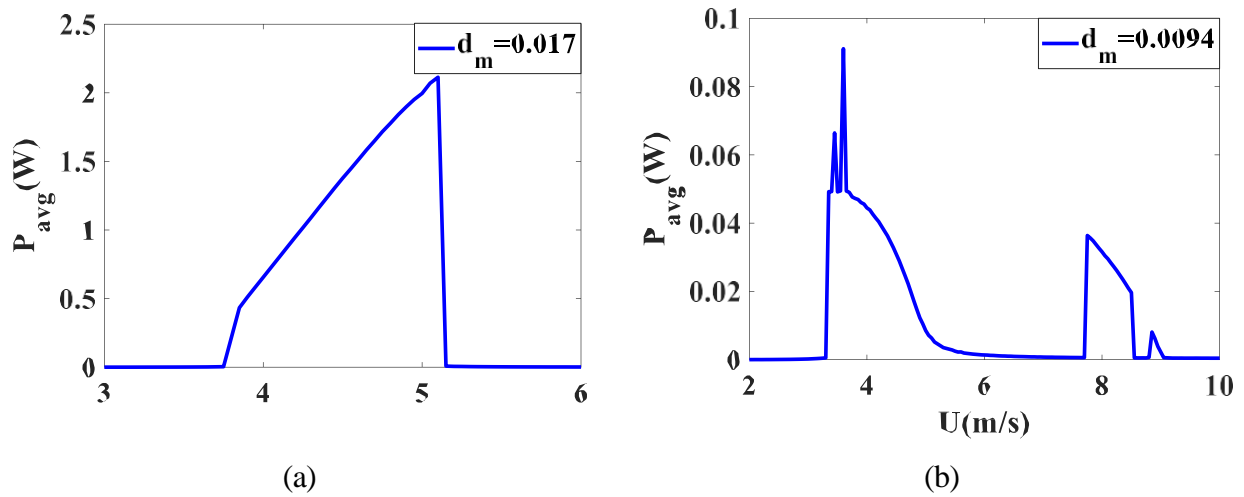(a)   (b)

Figure 4.10: Average harvested power at (a) d_m=1.7cm (mono-stable) (b) d_m=0.94cm (bi-stable)

4.5 Analysis at coupled frequency 80 rad/sec

In Figure 4.11, at a wind speed of about 4.6 m/s, the maximum value of gathered power reaches about 0.75 W. Initially, with wind speeds less than 4 m/s, the power stays extremely low and nearly constant. The power increases quickly and peaks dramatically at 4.6 m/s when the wind speed rises above 4 m/s. There is a sharp decline after reaching the apex, then some oscillations. The power steadily diminishes as the wind speed climbs above 5 m/s. The efficiency of energy harvesting reaches its peak at wind speeds of approximately 4.6 m/s, after which it starts to decrease.
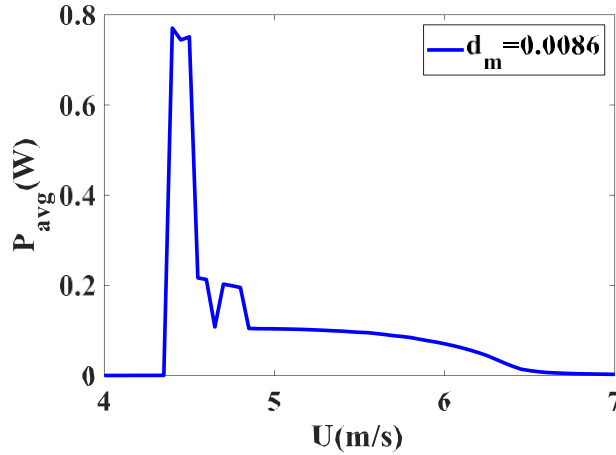
**Figure 4.11:** Average harvested power at d_m=0.86cm (bi-stable)

4.6 Analysis of displacement in both mono-stable and bi-stable states

Figure 4.12: (a) d_m = 1.7cm, 1.153cm, 1.072cm are the magnetic spacing for the mono-stable state. Overall spacing intervals, the displacement is insignificant at lower wind speeds (below 2m/s). The displacements begin to climb, albeit at different rates for each dm, as wind speed rises over 2m/s. d_m = 0.017cm: Shows the most pronounced displacement peak, which abruptly drops off after approaching 15mm at a wind speed of about 4.6 m/s. d_m = 0.01072cm and d_m = 0.01153cm. These layouts indicate low displacement for all wind speeds, with substantially smaller displacement values (under 5 mm) and very flat curves. For one of the states, the graph displays a sudden increase in displacement, suggesting that the mono-stable zone only produces significant displacement at specific wind speeds before steeply declining beyond a given threshold.

Figure 4.12: (b) d_m = 0.86cm, 0.94cm, 1.006cm, and 1.032cm are the magnetic spacing for the bi-stable state. Compared to the mono-stable situation, there is greater fluctuation in the displacements in the bi-stable area. As wind speed increases, the behaviour exhibits several peaks and irregularities in displacement, exhibiting significant variation over different dm values. d_m = 0.0086cm. This arrangement shows the most complex behaviour, which shows oscillations at increasing wind speeds after a significant peak at about 6 mm displacement at 4.6 m/s. d_m = 0.0094cm. displays two conspicuous peaks with displacements of around 6 mm, one at 4 m/s and the other at 6 m/s, followed by a continuous decline.dm = 0.01006cm and 0.01032cm. Show comparatively small displacement values (less than 3 mm) with variations between 3 and 6 m/s.

Comparing this line to that of $d_m = 0.0094$cm and $d_m = 0.0086$cm, it shows more abnormalities but less overall displacement. Compared to the mono-stable state, the bi-stable area is more sensitive to changes in wind speed due to its frequent displacement jumps, which reflect non-linear behaviour.
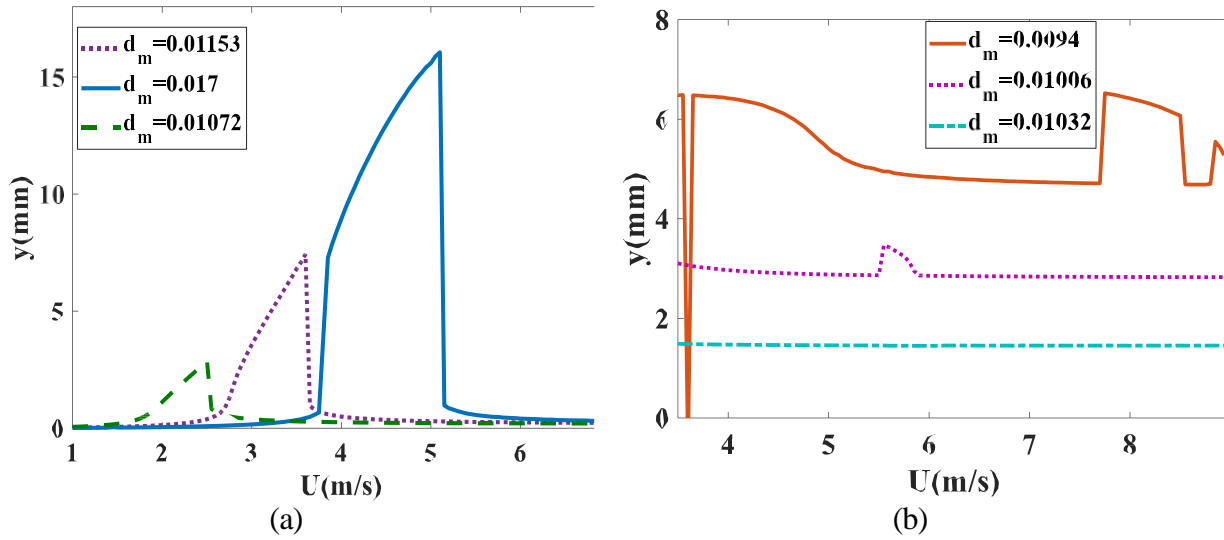
Figure 4.12: Displacement at (a) d_m=1.7cm, 1.153cm, 1.072cm (mono-stable) (b)0.94cm, 1.006cm, 1.032cm (bi-stable)

CHAPTER 5: CONCLUSION AND FUTURE WORK

5.1 Conclusion

The outcomes obtained from simulating the mathematical model served as the foundation for the performance analysis of the piezoelectric energy harvester. Both mono-stable and bi-stable versions of the piezoelectric energy harvester operating under the influence of VIV were examined in terms of performance and efficiency. The study was conducted at the same coupled frequency for mono-stable states and bi-stable states. For some d_m values, the mono-stable arrangement exhibits smoother, more predictable behaviour with a sharp displacement peak at higher wind speeds. The more complex dynamics at different wind speeds are reflected by the more irregular and oscillating displacement with many peaks and leaps in the bi-stable state. This behaviour might be a sign of less stable bi-stable systems with more potential for energy harvesting. For power, it can be observed that there is a single peak in the case of a mono-stable state, while in the case of bi-stable, it has multiple peaks and a broad wind speed range.

5.2 Recommendations for future work

In the modern era, small gadgets and sensors are used very often. The piezoelectric energy harvester can fulfill the needs of small gadgets used in various appliances. It has certain advantages as it will replace the batteries, and no fuel is required as a fundamental resource is used. Compared to batteries, it is a long-lasting and environmentally friendly system. There has been a lot of research on improving and optimizing piezoelectric energy harvesting. Yet, there are a lot of optimizations to be done to make it suitable for commercial use and global use.

a) Analysis of the piezoelectric energy harvester using vortex-induced vibration with base acceleration.
b) Analysis of the hybrid energy harvester after adding galloping and VIV to the base excitation. In that case, the phenomenon of unsteady galloping will become relevant.

REFERENCES

[1] Avtar, R., Sahu, N., Aggarwal, A. K., Chakraborty, S., Kharrazi, A., Yunus, A. P.,... & Kurniawan, T. A. (2019). Exploring renewable energy resources using remotesensing and GIS—A review. Resources, 8(3), 149.

[2] Nechibvute, A., Chawanda, A., & Luhanga, P. (2012). Piezoelectric energy harvesting devices: an alternative energy source for wireless sensors.Smart Materials Research, 2012.

[3] Chalasani, S., & Conrad, J. M. (2008, April). A survey of energy harvestingsources for embedded systems. In IEEE SoutheastCon 2008 (pp. 442-447). IEEE.

[4] Ferdous, R. M., Reza, A. W., & Siddiqui, M. F. (2016). Renewable energy harvesting for wireless sensors using passive RFID tag technology: A review. Renewable and Sustainable Energy Reviews, 58, 1114-1128.

[5] Yildiz, F. (2009). Potential Ambient Energy-Harvesting Sources and Techniques. Journal of technology Studies, 35(1), 40-48.

[6] Wang, Z. L., Jiang, T., & Xu, L. (2017). Toward the blue energy dream by triboelectric nanogenerator networks. Nano Energy, 39, 9-23.

[7] Ahmed, A., Hassan, I., Helal, A. S., Sencadas, V., Radhi, A., Jeong, C. K., & El- Kady, M. F. (2020). Triboelectric nanogenerator versus piezoelectric generator at low frequency (< 4 Hz): a quantitative comparison. Iscience, 23(7), 101286.

[8] Abdelkefi, A. (2016). Aeroelastic energy harvesting: A review. International Journal of Engineering Science, 100, 112-135.

[9] Abdelkefi, A. (2016). Aeroelastic energy harvesting: A review. International Journal of Engineering Science, 100, 112-135.

[10] Shaikh, F. K., & Zeadally, S. (2016). Energy harvesting in wireless sensor networks: A comprehensive review. Renewable and Sustainable Energy Reviews, 55, 1041-1054

[11] Amin Karami, M., & Inman, D. J. (2012). Powering pacemakers from heartbeat vibrations using linear and nonlinear energy harvesters. Applied Physics Letters, 100(4), 042901.

[12] Alam, M., Li, S., Ahmed, R. U., Yam, Y. M., Thakur, S., Wang, X. Y., ... Zheng, Y. P. (2019). Development of a battery-free ultrasonically powered functional electrical stimulator for movement restoration after paralyzing spinal cord injury. Journal of

neuroengineering and rehabilitation, 16(1), 1-14.

[13] Muralt, P. (2000). Ferroelectric thin films for micro-sensors and actuators: a review. Journal of micromechanics and microengineering, 10(2), 136.

[14] Lu, Z. Q., Zhao, L., Ding, H., & Chen, L. Q. (2021). A dual-functional metamaterial for integrated vibration isolation and energy harvesting. Journal of Sound and Vibration, 509, 116251.

[15] Butt, Z., Pasha, R. A., Qayyum, F., Anjum, Z., Ahmad, N., & Elahi, H. (2016). Generation of electrical energy using lead zirconate titanate (PZT-5A) piezoelectric material: Analytical, numerical and experimental verifications. Journal of Mechanical Science and Technology, 30(8), 3553-3558.

[16] Khan, M. U., Butt, Z., Elahi, H., Asghar, W., Abbas, Z., Shoaib, M., & Bashir, M. (2019). Deflection of coupled elasticity–electrostatic bimorph PVDF material: theoretical, FEM and experimental verification. Microsystem Technologies, 25(8), 3235-3242.

[17] Khan, F. U., & Qadir, M. U. (2016). State-of-the-art in vibration-based electrostatic energy harvesting. Journal of Micromechanics and Microengineering, 26(10), 103001

[18] Anton, S. R., & Sodano, H. A. (2007). A review of power harvesting using piezoelectric materials (2003–2006). Smart materials and Structures, 16(3), R1.

[19] Abdelkefi, A. (2016). Aeroelastic energy harvesting: A review. International Journal of Engineering Science, 100, 112-135.

[20] Mallick, D., Amann, A., & Roy, S. (2014). A nonlinear stretching based electromagnetic energy harvester on FR4 for wideband operation. Smart Materials and Structures, 24(1), 015013.

[21] Kim, H. S., Kim, J. H., & Kim, J. (2011). A review of piezoelectric energy harvesting based on vibration. International journal of precision engineering and manufacturing, 12(6), 1129-1141.

[22] Erturk, A. (2009). Electromechanical modeling of piezoelectric energyharvesters (Doctoral dissertation, Virginia Tech).

[23] Kim, M., Ito, R., Kim, S., Khanal, G. P., Fujii, I., Suzuki, T. S., ... & Wada, S.(2018).Fabrication of lead-free piezoelectric (Bi0. 5Na0. 5) TiO3–BaTiO3 ceramics using electrophoretic deposition. Journal of Materials Science, 53(4), 2396-2404.

[24] Kim, M., Ito, R., Kim, S., Khanal, G. P., Fujii, I., Suzuki, T. S., ... & Wada, S.(2018).Fabrication of lead-free piezoelectric (Bi0. 5Na0. 5) TiO3–BaTiO3 ceramics using electrophoretic deposition. Journal of Materials Science, 53(4), 2396-2404.

[25] Yuan, T. C., Yang, J., & Chen, L. Q. (2018). Nonlinear dynamics of a circular piezoelectric plate for vibratory energy harvesting. Communications in Nonlinear Science and Numerical Simulation, 59, 651-656.

[26] Saoutieff, E., Allain, M., Nowicki-Bringuier, Y. R., Viana, A., & Pauliac-Vaujour, E. (2016). Integration of piezoelectric nanowires matrix onto a microelectronics chip. Procedia Engineering, 168, 1638-1641.

[27] Kim, H. S., Kim, J. H., & Kim, J. (2011). A review of piezoelectric energy harvesting based on vibration. International journal of precision engineering and manufacturing, 12(6), 1129-1141.

[28] Safaei, M., Sodano, H. A., & Anton, S. R. (2019). A review of energy harvesting using piezoelectric materials: state-of-the-art a decade later (2008–2018). Smart Materials and Structures, 28(11), 113001.

[29] S. Radkowski, K. Lubikowski, A. Pietak, Vibration Energy Harvesting in the Transportation System : A Review, Diagnostyka - Appl. Struct. Heal. Usage Cond. Monit. 4 (2012) 39–44.

[30] S. Radkowski, K. Lubikowski, A. Pietak, Vibration Energy Harvesting in the Transportation System : A Review, Diagnostyka - Appl. Struct. Heal. Usage Cond. Monit. 4 (2012) 39–44.

[31] S. Radkowski, K. Lubikowski, A. Pietak, Vibration Energy Harvesting in the Transportation System : A Review, Diagnostyka - Appl. Struct. Heal. Usage Cond. Monit. 4 (2012) 39–44.

[32] E. Blokhina, A. El Aroudi, E. Alarcon, D. Galayko, Introduction to vibration energy harvesting, Nonlinearity Energy Harvest. Syst. Micro- Nanoscale Appl. (2016) 1–21. https://doi.org/10.1007/978-3-319-20355-3_1.

[33] D. Zhu, S. Beeby, Kinetic energy harvesting, Energy Harvest. Syst. Princ. Model. Appl. (2011) 1–77. https://doi.org/10.1007/978-1-4419-7566-9_1.

[34] M. Safaei, H.A. Sodano, S.R. Anton, A review of energy harvesting using piezoelectric materials: State-of-the-art a decade later (2008-2018), Smart Mater. Struct. 28 (2019). https://doi.org/10.1088/1361-665X/ab36e4.

[35] A. Abdelkefi, A.H. Nayfeh, M.R. Hajj, M.R. Paul, C. a Woolsey, Global Nonlinear Analysis of Piezoelectric Energy Harvesting from Ambient and Aeroelastic Vibrations Global Nonlinear Analysis of Piezoelectric Energy Harvesting from Ambient and Aeroelastic Vibrations Abdessattar Abdelkefi (ABSTRACT), (2012).

[36] Y.J. Lee, Y. Qi, G. Zhou, K.B. Lua, Vortex-induced vibration wind energy harvesting by piezoelectric MEMS device in formation, Sci. Rep. 9 (2019) 1–11. https://doi.org/10.1038/s41598-019-56786-0.

[37] R. Naseer, H.L. Dai, A. Abdelkefi, L. Wang, On the potential of mono-stable piezomagnetoelastic energy harvesting from vortex-induced vibrations, 58th AIAA/ASCE/AHS/ASC Struct. Struct. Dyn. Mater. Conf. 2017 (2017). https://doi.org/10.2514/6.2017-0626.

[38] H.L. Dai, A. Abdelkefi, U. Javed, L. Wang, Modeling and performance of electromagnetic energy harvesting from galloping oscillations, Smart Mater. Struct. 24 (2015). https://doi.org/10.1088/0964-1726/24/4/045012.

[39] A.H. Alhadidi, M.F. Daqaq, A broadband bi-stable flow energy harvester based on the wake-galloping phenomenon, Appl. Phys. Lett. 109 (2016). https://doi.org/10.1063/1.4959181.

[40] S.R. Anton, H.A. Sodano, A review of power harvesting using piezoelectric materials (2003-2006), Smart Mater. Struct. 16 (2007) 197–205. https://doi.org/10.1088/0964-1726/16/3/R01.

[41] S. Zheng, M. Chen, Z. Li, H. Wang, Size-dependent constituent equations of piezoelectric bimorphs, Compos. Struct. 150 (2016) 1–7. https://doi.org/10.1016/j.compstruct.2016.04.039.

[42] A. Naqvi, A. Ali, W.A. Altabey, S.A. Kouritem, Energy Harvesting from Fluid Flow Using Piezoelectric Materials: A Review, Energies 15 (2022). https://doi.org/10.3390/en15197424.

[43] W. Chen, X. Li, W. Yang, Shape optimization to enhance energy harvesting from vortex-induced vibration of a circular cylinder, Phys. Fluids 36 (2024). https://doi.org/10.1063/5.0189915.

[44] L. Zhao, J. Chong, T.L.J. Ng, Y. Yang, Enhancement of aeroelastic energy harvesting from galloping, vortex-induced vibrations and flutter with a beam stiffener, ICAST 2014 - 25th Int. Conf. Adapt. Struct. Technol. (2014). https://doi.org/10.13140/2.1.4450.6404.

[45] R.C. Sugato Hajra, Arya Tripathy, Basanta K Panigrahi, ce pte d M pt, Nanotechnology 29 (2019) 465705.

[46] R.C. Sugato Hajra, Arya Tripathy, Basanta K Panigrahi, ce pte d M pt, Nanotechnology 29 (2019) 465705.

[47] Yildirim, T., Ghayesh, M. H., Li, W., & Alici, G. (2016). A review on performance enhancement techniques for ambient vibration energy harvesters. Renewable and Sustainable Energy Reviews.

[48] Pellegrini, S. P., Tolou, N., Schenk, M., & Herder, J. L. (2013). Bi-stable vibration energy harvesters: a review. Journal of Intelligent Material Systems and Structures, 24(11), 1303-1312.

[49] Amin Karami, M., & Inman, D. J. (2012). Powering pacemakers from heartbeat vibrations using linear and nonlinear energy harvesters. Applied Physics Letters, 100(4), 042901.

[50] Wang, J., Hu, G., Su, Z., Li, G., Zhao, W., Tang, L., & Zhao, L. (2019). A cross-coupled dual-beam for multi-directional energy harvesting from vortex induced vibrations. Smart Materials and Structures, 28(12), 12LT02.

[51] Zou, H. X., Zhao, L. C., Gao, Q. H., Zuo, L., Liu, F. R., Tan, T., ... & Zhang, W. M. (2019). Mechanical modulations for enhancing energy harvesting: Principles, methods and applications. Applied Energy, 255, 113871.

[52] Wang, J., Geng, L., Ding, L., Zhu, H., & Yurchenko, D. (2020). The state-of-the- art review on energy harvesting from flow-induced vibrations. Applied Energy, 267, 114902.

[53] Naseer, R., Dai, H., Abdelkefi, A., & Wang, L. (2019). Comparative study of piezoelectric vortex-induced vibration-based energy harvesters with multi- stability characteristics. Energies, 13(1), 71.

[54] Naseer, R., Dai, H. L., Abdelkefi, A., & Wang, L. J. A. E. (2017). Piezomagnetoelastic energy harvesting from vortex-induced vibrations using mono-stable characteristics. Applied Energy, 203, 142-153.

[55] Zhao, L., & Yang, Y. (2018). An impact-based broadband aeroelastic energy harvester for concurrent wind and base vibration energy harvesting. Applied energy, 212, 233-243.

[56] Zhao, L. (2020). Synchronization extension using a bi-stable galloping oscillator for enhanced power generation from concurrent wind and base vibration. Applied Physics Letters, 116(5), 053904.

[57] Alam, M., Li, S., Ahmed, R. U., Yam, Y. M., Thakur, S., Wang, X. Y., ... Zheng, Y. P. (2019). Development of a battery-free ultrasonically powered functional electrical stimulator for movement restoration after paralyzing spinal cord injury. Journal of neuroengineering and rehabilitation, 16(1), 1-14.

[58] Zhang, L. B., Abdelkefi, A., Dai, H. L., Naseer, R., & Wang, L. (2017). Design and experimental analysis of broadband energy harvesting from vortex-induced vibrations. Journal of Sound and Vibration, 408, 210-219.

[59] Zhou, S., Cao, J., Inman, D. J., Lin, J., Liu, S., & Wang, Z. (2014). Broadband tristable energy harvester: modeling and experiment verification. Applied Energy, 133, 33-39.

[60] Facchinetti ML, de Langre E, Biolley F. Coupling of structure and wake oscillators in vortex-induced vibrations. J Fluids Struct 2004;19:123–40.

[61] Violette R, De Langre E, Szydlowski J. Computation of vortex-induced vibrations of long structures using a wake oscillator model: comparison with DNS and experiments. Comput Struct 2007;85(11):1134–41.

[62] Akaydin HD, Elvin N, Andreopoulos Y. The performance of a self-excited fluidic energy harvester. Smart Mater Struct 2012;21:025007.

[63] Harne RL, Wang KW. A review of the recent research on vibration energy harvesting via bi-stable systems. Smart Mater Struct 2013;22(2):023001.

[64] R. Naseer, H. Dai, A. Abdelkefi, and L. Wang, "On the potential of mono-stable piezomagnetoelastic energy harvesting from vortex-induced vibrations," in 58th AIAA/ASCE/AHS/ASC Structures, Structural Dynamics, and Materials Conference, 2017, p. 0626.

[65] Rao, B. D., & Arun, K. S. (1992). Model-based processing of signals: A state space approach. Proceedings of the IEEE, 80(2), 283-309.